arXiv:astro-ph/9802109v2 28 Aug 1998

Joint estimation of cosmological parameters from CMB and IRAS data

Matthew Webster[1]
Institute of Astronomy, Madingley Road, Cambridge CB3 0HA, UK

S.L. Bridle, M.P. Hobson and A.N. Lasenby
Astrophysics Group, Cavendish Laboratory, Madingley Road, Cambridge CB3 0HE, UK

Ofer Lahav
Institute of Astronomy, Madingley Road, Cambridge CB3 0HA, UK

and

Graça Rocha
Department of Physics, Kansas State University, Manhattan, KS 66506, USA

ABSTRACT

Observations of large scale structure (LSS) and the Cosmic Microwave Background (CMB) each place separate constraints on the values of cosmological parameters. We calculate a joint likelihood based on various CMB experiments and the IRAS 1.2Jy galaxy redshift survey and use this to find an overall optimum with respect to the free parameters. Our formulation self-consistently takes account of the underlying mass distribution, which affects both the CMB potential fluctuations and the IRAS redshift distortion. This not only allows more accurate parameter estimation, but also removes the parameter degeneracy which handicaps calculations based on either approach alone. The family of Cold Dark Matter (CDM) models analysed corresponds to a spatially-flat universe with an initially scale-invariant spectrum and a cosmological constant. Free parameters in the joint model are the mass density due to all matter ($\Omega_{\rm m}$), Hubble's parameter ($h = H_0/100$ km s^{-1}Mpc^{-1}), the quadrupole normalisation of the CMB power spectrum (Q) in μK, and the IRAS light-to-mass bias ($b_{\rm iras}$). Throughout the analysis, the baryonic density (Ω_b) is required is to satisfy the nucleosynthesis constraint $\Omega_b h^2 = 0.024$. Results from the two data sets show good agreement, and the joint optimum lies at $\Omega_{\rm m} = 0.39$, $h = 0.53$, $Q = 16.96$ μK, and $b_{\rm iras} = 1.21$. The 68 per cent confidence intervals are: $0.29 < \Omega_{\rm m} < 0.53$, $0.39 < h < 0.58$, $15.34 < Q < 17.60$, and $0.98 < b_{\rm iras} < 1.56$. For the above parameters the normalisation and shape of the mass power-spectrum are $\sigma_8 = 0.67$ and $\Gamma = 0.15$, and the age of the Universe is 16.5 Gyr.

Subject headings: Cosmic microwave background, Large-scale structure

[1]email: mwebster@ast.cam.ac.uk

1. Introduction

Astronomical observations allow us to evaluate cosmological models, and determine likely values for the parameters within them. As the variety and depth of these observations have improved, so too have the techniques for comparing them against theoretical predictions.

Observations of anisotropies in the Cosmic Microwave Background (CMB) provide one of the key constraints for cosmological models and a significant quantity of experimental data already exists. By comparing the power spectrum of the CMB fluctuations derived from these experiments with the power spectra predicted by different cosmological models it is possible to set constraints on the value of certain cosmological parameters (e.g. Hancock et al. 1998, Lineweaver et al. 1997, and references therein).

Galaxy redshift surveys, mapping large scale structure (LSS), provide another cosmologically important set of observations. The clustering of galaxies in redshift-space is systematically different from that in real-space (Kaiser 1987). The mapping between the two is a function of the underlying mass distribution, in which the galaxies are not only tracers, but also velocity test particles (Lahav 1996). Many techniques have been developed for estimating this mapping (Yahil et al. 1991, Kaiser et al. 1991). Statistical quantities can be generated for a given cosmology and these used to constrain model parameters through comparison with survey data (Fisher, Scharf & Lahav 1994, Cole et al. 1995, Heavens & Taylor 1995, Fisher & Nusser 1996, Willick et al. 1997).

Estimates derived separately from each of these two data sets have problems with parameter degeneracy. In the analysis of LSS data, there is uncertainty as to how well the observed light distribution traces the underlying mass distribution. The light-to-mass linear bias, b, introduced to account for this uncertainty, affects the value of many central cosmological parameters, and makes any identified optimum degenerate (Strauss & Willick 1995). Similarly, on the basis of CMB data alone, there is considerable degeneracy (Bond et al. 1995c) between $h = H_0/100$ km s^{-1}Mpc^{-1} and the energy density Ω_Λ due to the cosmological constant (Carroll, Press & Turner 1992). This leads to poor estimation of the baryon ($\Omega_{\rm b}$) and total mass ($\Omega_{\rm m}$) densities (Lineweaver et al. 1997).

In this letter, we combine results from a bandpower approach covering a range of CMB experiments, with a likelihood analysis of the IRAS 1.2Jy survey, performed in spherical harmonics. We present a self-consistent formulation of CMB and LSS parameter estimation. In particular, our method expresses the effects of the underlying mass distribution on both the CMB potential fluctuations and the IRAS redshift distortion. This breaks the degeneracy inherent in an isolated analysis of either data set, and places tight constraints on several cosmological parameters. Indeed, it is unsurprising that the two data sets are complementary, given that they sample our universe at extreme ends of its evolution. For simplicity, we restrict our attention to inflationary, Cold Dark Matter (CDM) models, assuming a flat universe with linear, scale-independent biasing. Other recent studies which combine CMB and LSS include Gawiser & Silk 1998 and Eisenstein, Hu & Tegmark 1998.

2. CMB Parameter Estimation

2.1. Experimental Data

Since the discovery of CMB fluctuations by the COBE satellite (Smoot et al. 1992, Bennett et al. 1996), several other experiments have also measured CMB anisotropies over a wide range of angular scales. These experiments include ground-based beam-switching experiments such as Tenerife (Hancock et al. 1997, Hancock et al. 1994), Python (Ruhl et al. 1995), South Pole (Gundersen et al. 1995) and Saskatoon (Netterfield et al. 1997); balloon-borne instruments such as ARGO (De Bernardis et al. 1994), MAX (Tanaka et al. 1996), and MSAM (Cheng et al. 1994, Cheng et al. 1996) and the ground-based interferometers CAT (Scott et al. 1996) and OVRO (Leitch et al. 1998).

These observations have resulted in a first estimate of the CMB power spectrum and they are discussed in more detail by Hancock et al. 1998. In particular, Hancock et al. display the window function W_l for each experiment and convert the level of anisotropy observed in each case to flat bandpower estimates $(\Delta T_l/T) \pm \sigma$ centered on the effective multipole $l_{\rm eff}$ of the corresponding window function (see below). The resulting CMB data points are plotted in Fig. 1, together with their 68 per cent confidence limits. These confidence limits have been obtained using likelihood analyses and hence incorporate uncertainties due to random errors, sampling variance (Scott, Srednicki and White 1994) and cosmic variance (Scaramela & Vittorio 1990, Scaramela & Vittorio 1993). A discussion of possible additional uncertainties due to contamination by foreground emission is given by Rocha et al. 1998.

The data points plotted in Fig. 1 differ slightly from those given in Hancock et al. 1998 as follows. The old Python point has been replaced by two new points corresponding to the Py III_S and Py I, Py II and Py III_L observations respectively (Platt et al. 1997). The Tenerife point has been updated following the analysis of the full two-dimensional data-set and a detailed treatment of atmospheric effects (Gutierrez 1997). The Saskatoon points have been increased by 5 per cent, as suggested by the recent investigation of systematic calibration errors in the Saskatoon experiment (Leitch, private communication). We have added the results from the second CAT field, reported in Baker et al. 1998 and also the OVRO point reported by Leitch et al. 1998.

2.2. Method

Temperature fluctuations in the CMB are usually described in terms of the spherical harmonic expansion

$$\frac{\Delta T(\theta,\phi)}{T} = \sum_{l=0}^{\infty} \sum_{m=-l}^{l} a_{lm}\, Y_{lm}(\theta,\phi) \ , \qquad (1)$$

from which we define the ensemble-average CMB power spectrum $C_l = \langle |a_{lm}|^2 \rangle$. Alternatively, we may describe the fluctuations in terms of their autocorrelation function

$$C(\theta) = \frac{1}{4\pi} \sum_{l=2}^{\infty} (2l+1)\, C_l\, P_l(\cos\theta) \ . \tag{2}$$

The power in the CMB fluctuations observed by an experiment with window function W_l is then given by

$$C_{\rm obs}(0) = \left\langle \left(\frac{\Delta T_{\rm obs}}{T} \right)^2 \right\rangle = \frac{1}{4\pi} \sum_{l=2}^{\infty} (2l+1)\, C_l\, W_l \ , \tag{3}$$

and for each experiment we define the flat bandpower by

$$\frac{\Delta T_l}{T} = \sqrt{\frac{C_{\rm obs}(0)}{I(W_l)}} \ , \tag{4}$$

where $I(W_l)$ is defined (Bond 1995*a*, Bond 1995*b*) as

$$I(W_l) = \sum_{l=2}^{\infty} \frac{(l+\frac{1}{2})}{l\,(l+1)}\ W_l \ . \tag{5}$$

This flat bandpower estimate is centred on the effective multipole

$$l_{\rm eff} = \frac{I(l\, W_l)}{I(W_l)} \ . \tag{6}$$

We wish to compare these bandpower estimates with those predicted by different cosmological models. Varying the values of model parameters, we calculate corresponding, predicted CMB power spectrum C_l, using the Boltzmann code of Seljak & Zaldarriaga 1996. This is then used to calculate the predicted flat bandpower ΔT_l for each experiment. The chi-squared statistic for a given set of parameter values, $\vec{\alpha}_{\rm cmb}$, is then

$$\chi^2(\vec{\alpha}_{\rm cmb}) = \sum_{i=1}^{N_{\rm d}} \frac{1}{\sigma_i^2} \Big(\Big[\Delta T_l^{\rm obs} \Big]_i - \Big[\Delta T_l^{\rm pred}(\vec{\alpha}_{\rm cmb}) \Big]_i \Big)^2 \ , \tag{7}$$

where $N_{\rm d}$ is the number of CMB data points plotted in Fig. 1 (20 in this analysis). Moreover, since the CMB data points plotted in Fig. 1 were chosen such that no two bandpower estimates come from experiments which observed overlapping patches of sky and had overlapping window functions, we may consider them as *independent* estimates of the CMB power spectrum. As the cosmic variance has already been taken into account in deriving the flat bandpower estimates, the likelihood function is given simply by $\mathcal{L}_{\rm cmb} \propto e^{-\chi^2/2}$.

As mentioned above, we assume that the Universe is spatially flat, and that there are no tensor contributions to the CMB power spectrum. We take the primordial scalar perturbations to be described by the Harrison-Zel'dovich power spectrum for which $n_{\rm s} = 1$, and further assume that the optical depth to the last scattering surface is zero.

The normalisation of the CMB power spectrum is determined by Q, which gives the strength of the quadrupole in μK, such that

$$C_2 = \frac{4\pi}{5}\left(\frac{Q}{T_0}\right)^2 , \tag{8}$$

where T_0 is the average CMB temperature. The expansion rate of the Universe is given by Hubble's parameter $h = H_0/100$ km s^{-1}Mpc^{-1}, while $\Omega_{\rm cdm}$ and $\Omega_{\rm b}$ denote the density of the Universe in CDM and the baryons respectively, each in units of the critical density. Given that we assume a flat universe, but investigate models where

$$\Omega_{\rm m} \equiv (\Omega_{\rm cdm} + \Omega_{\rm b}) < 1 , \tag{9}$$

the shortfall is made up through a non-zero cosmological constant Λ such that

$$\Omega_\Lambda = 1 - \Omega_{\rm m} = \frac{\Lambda}{3H_0^2} . \tag{10}$$

Furthermore, we restrict our attention to models that satisfy the nucleosynthesis constraint $\Omega_b h^2 = 0.024$ (Tytler, Fan & Burles 1996). Thus we consider the reduced set of CMB parameters

$$\vec{\alpha}_{\rm cmb} \equiv \{Q, h, \Omega_{\rm cdm}\} . \tag{11}$$

In Section 4, we derive a set of joint parameters linking these to the IRAS parameter set.

3. IRAS Parameter Estimation

3.1. IRAS 1.2Jy Survey

The IRAS surveys are uniform and complete down to Galactic latitudes as low as $\pm 5^\circ$ from the Galactic plane. This makes them ideal for estimating whole-sky density and velocity fields. Here, we use the 1.2 Jy IRAS survey (Fisher et al. 1995), consisting of 5313 galaxies, covering 87.6% of the sky with the incomplete regions being dominated by the 8.7% of the sky with $|b| < 5^\circ$.

In principle, the method we are using can be extended to account explicitly for the incomplete sky coverage. However, we adopt the simpler approach of smoothly interpolating the redshift distribution over the missing areas (Yahil et al. 1991). The effects of this interpolation on the computed harmonics have been shown to be negligible (Lahav et al. 1994).

3.2. Method

In this letter, we assume linear, scale-independent biasing, where $b_{\rm iras}$ measures the ratio between fluctuations in the IRAS galaxy distribution and the underlying mass density field:

$$(\delta\rho/\rho)_{\rm iras} = b_{\rm iras}\,(\delta\rho/\rho)_{\rm m} . \tag{12}$$

We note that biasing may be non-linear, stochastic, non-local, scale-dependent, epoch-dependent and type-dependent (e.g. Dekel and Lahav 1998, Tegmark & Peebles 1998, Pen 1998, Bagla 1998, Blanton et al. 1998, and references therein). For a linear bias parameter, $b_{\rm iras}$, the velocity and density fields in linear theory (Peebles 1980) are linked by a proportionality factor $\beta_{\rm iras} \equiv {\Omega_{\rm m}}^{0.6}/b_{\rm iras}$, such that

$$\nabla \cdot \mathbf{v} = -H_0 \, \beta_{\rm iras} \, \left(\delta\rho/\rho\right)_{\rm m} \tag{13}$$

Statistically, the fluctuations in the real-space galaxy distribution can be described by a power spectrum, $P_{\rm R}(k)$, which is determined by the *rms* variance in the observed galaxy field, measured for an 8 h^{-1}Mpc radius sphere ($\sigma_{8,\rm iras}$) and a shape parameter (e.g. Γ in equation 19). The observed $\sigma_{8,\rm iras}$ is related to the underlying σ_8 for mass through the bias parameter, such that $\sigma_{8,\rm iras} = b_{\rm iras}\,\sigma_8$.

The approach we use in this letter follows Fisher, Scharf & Lahav (1994; hereafter FSL), and we include here only a brief introduction to our technique. FSL provides a detailed description of the spherical harmonic approach to parameter estimation. A flux-limited, redshift-space density field can be decomposed into spherical harmonics Y_{lm}, with coefficients

$$a^{\rm S}_{lm} = \sum_{i=1}^{N_{\rm g}} f(s_i)\, Y_{lm}\left(\hat{\mathbf{s}}_i\right) \ , \tag{14}$$

where $N_{\rm g}$ is the number of galaxies in the survey, and $f(s)$ is an arbitrary radial weighting function—this process is analogous to Fourier decomposition, but instead using spherical basis functions. The sum over galaxies in this equation can be rewritten as a continuous integral of the density fluctuation field $\delta(\mathbf{s})$ over redshift-space:

$$a^{\rm S}_{lm} = \int d^3\mathbf{s} \ \phi(r)\, f(s) \ \left[1 + \delta_S(\mathbf{s})\right] \ Y_{lm}(\hat{\mathbf{s}}) \ , \tag{15}$$

where $\phi(r)$ is the radial selection function of the survey, evaluated at the real-space distance of the $i^{\rm th}$ galaxy.

As detailed in FSL, assuming the perturbations introduced by peculiar velocities are small, the expected linear theory values for the harmonic coefficients are

$$\left\langle \left| a^{\rm S}_{lm} \right|^2 \right\rangle_{\rm LT} = \frac{2}{\pi} \int_0^\infty dk \ k^2 \, P_{\rm R}(k) \left| \Psi^{\rm R}_l(k) + \beta_{\rm iras} \Psi^{\rm C}_l(k) \right|^2 \ . \tag{16}$$

Here, $\Psi^{\rm R}$ is the real-space window function, while $\beta_{\rm iras}\Psi^{\rm C}$ is a "correction" term which embodies the redshift distortion.

For a given set of cosmological parameters, redshift-space harmonics a^j_{lm} can be calculated for different weighting functions $f^j(r)$, $j = 1, ..., N$. If the underlying density field is Gaussian, on the basis of the coefficients predicted in equation 16, the likelihood of the survey harmonics can be calculated as

$$\mathcal{L}_{\rm iras} \propto |\mathbf{A}|^{-\frac{1}{2}} \exp\left(-\frac{1}{2} \left[\vec{a}^{\rm T} \, \mathbf{A}^{-1} \, \vec{a} \right] \right) \ . \tag{17}$$

Here $\vec{a}$ is the vector of observed harmonics for different shells and $\mathbf{A}$ is the corresponding covariance matrix, which depends on the predicted harmonics. In addition to the $\langle|a^{\rm S}_{lm}|\rangle_{\rm LT}$ from equation 16, these predicted harmonics will also have a shot-noise contribution $\langle|a^{\rm S}_{lm}|\rangle_{\rm SN}$ due to the discreteness of survey galaxies. Note that the argument of the exponent in equation 17 is simply $(-\chi^2/2)$, and that here the normalisation of the likelihood function does depend on the free parameters (unlike in the CMB likelihood function).

In this letter, we follow FSL and use four Gaussian windows centered at 38, 58, 78, and 98 h^{-1}Mpc each with a dispersion of 8 h^{-1}Mpc. For each window, we compute the corresponding weighted redshift harmonics for the IRAS 1.2Jy catalog, and use these to determine the likelihood of a given set of parameter values. Since our analysis is valid only in the linear regime, we restrict the likelihood computation to $l_{\rm max} = 10$ (corresponding to 120 degrees of freedom). Hence, the IRAS likelihood function has a parameter vector

$$\vec{\alpha}_{\rm iras} \equiv \{\beta_{\rm iras}, \sigma_{8,\rm iras}, \Gamma\} \ . \tag{18}$$

Again, the linkage between these and the CMB parameters is discussed in section 4 below.

4. Joint analysis

Given the large number of parameters available between the two models, it is important both to find links for joint optimisation, and to decide which parameters can be frozen. From section 3, we have six variables between the two models: $\{Q,\ h,\ \Omega_{\rm cdm},\ \beta_{\rm iras},\ \sigma_{8,\rm iras},\ \Gamma\}$. These can be reduced further by expression in terms of core cosmological parameters. The IRAS normalisation can be calculated as $\sigma_8 \equiv f(\Omega_{\rm m}, Q, \Gamma)$ (Bardeen et al. 1986, Efstathiou, Bond & White 1995), while the CDM shape parameter is well approximated (Sugiyama 1995) by

$$\Gamma = \Omega_{\rm m}\, h\, \exp\left(-\Omega_{\rm b}\left[1 + \frac{\sqrt{h/0.5}}{\Omega_{\rm m}}\right]\right) \ . \tag{19}$$

Meanwhile, we have shown above that $\Omega_{\rm m} = \Omega_{\rm cdm} + \Omega_{\rm b}$, $\beta_{\rm iras} = \Omega_{\rm m}^{0.6}/b_{\rm iras}$, and $\sigma_{8,\rm iras} = \sigma_8 b_{\rm iras}$. Hence, the final, joint parameter space is

$$\vec{\alpha}_{\rm joint} \equiv \{h, Q, \Omega_{\rm m}, b_{\rm iras}\} \ . \tag{20}$$

As the IRAS and CMB probe very different scales and hence are assumed to be uncorrelated, the joint likelihood is given by

$$\ln\left(\mathcal{L}_{\rm joint}\right) = \ln\left(\mathcal{L}_{\rm cmb}\right) + \ln\left(\mathcal{L}_{\rm iras}\right) \ . \tag{21}$$

5. Results

The complementary nature of the two data sets is demonstrated in Fig. 2, which shows likelihood contours in the $\{\Omega_{\rm m},\ h\}$-plane after marginalising over Q and $b_{\rm iras}$. The fundamental

CMB-side degeneracy in $\{\Omega_{\rm m},\, h\}$ is seen in the flat trough running across Fig. 2a. The IRAS degeneracy is in a different direction (Fig. 2b) and the two data sets agree well in the region where the lines of degeneracy overlap. Combining the two data sets breaks the degeneracy and leads to a well defined joint optimum (Fig. 2c). The joint CMB plus IRAS likelihood function in the $\{\Omega_{\rm m},\, Q\}$-plane and $\{h,\, Q\}$-plane is plotted in Figs 3 & 4 respectively. In each case, a marginalisation has been performed over the other two parameters.

The joint likelihood (equation 21) was maximized with respect to the 4 free parameters (equation 20) using standard optimisation techniques (Press et al. 1992) and the best fit parameters are shown in Table 1. For this set of parameters, we find the values of the reduced χ^2 for the IRAS and CMB data respectively to be 1.18 and 1.03, confirming that both data-sets agree well with the models used. Taking the CMB and IRAS data together the total reduced χ^2 is 1.16. Recalculating the joint optimum using the simpler formula $\Gamma = \Omega_{\rm m}\, h$ in place of that in equation 19 had little effect. Further, the optimum was robust to changes in IRAS $l_{\rm max}$ in the range $4 \leq l_{\rm max} \leq 10$.

To obtain 68 per cent confidence limits on each of the free parameters it is necessary to marginalise over the remaining free parameters. To achieve this we evaluated the joint likelihood function on a 4-dimensional grid of parameter values. The range of values and number of grid points in each direction were $5 < Q < 30$, 50 steps; $0.3 < h < 0.9$, 50 steps; $0.1 < \Omega_{\rm m} < 1.0$, 100 steps; $0.7 < b_{\rm iras} < 2.0$, 20 steps. For each parameter, the corresponding one-dimensional marginalised probability distribution was calculated by integrating the likelihood function over the other variables. The marginalised distribution for each parameter is shown in Fig. 5, in which the dashed vertical lines denote the 68% confidence limits quoted in Table 1. In general, the peak of the one-dimensional probability distribution for each variable will differ from the global optimum across all parameters. However, for all four variables in this system, the two values are found to be extremely close.

In addition we evaluated the covariance matrix at the joint optimum. The covariance matrix is simply the inverse of the Hessian at the joint optimum. The Hessian is given by $\partial^2 \ln\left(\mathcal{L}_{\rm joint}\right)/(\partial\alpha_i \partial\alpha_j)$ for pairs of parameters α_i and α_j and is evaluated using a standard central-difference algorithm. Taking the square-root of the diagonal elements of the covariance matrix, the standard errors on the parameters are found to be $\Delta Q = 0.67\ \mu$K, $\Delta h = 0.03$, $\Delta\Omega_{\rm m} = 0.04$ and $\Delta b_{\rm iras} = 0.1$. Comparing these with the marginalised errors quoted in Table 1 we note that the marginalised errors are consistently larger, as expected. By rescaling the covariance matrix so that its diagonal elements equal unity, we obtain the correlation matrix shown in Table 2. We see that the most strongly correlated parameters are $\Omega_{\rm m}$ and h.

6. Discussion

The results of this joint optimisation are in reasonable agreement with other current estimates. The relatively low value of $\Omega_{\rm m} \approx 0.4$ is close to that found by others (White et al. 1993, Bahcall,

	Free parameters	
$\Omega_{\rm m}$	0.39	$0.29 < \Omega_{\rm m} < 0.53$
h	0.53	$0.39 < h < 0.58$
Q (μK)	16.95	$15.34 < Q < 17.60$
$b_{\rm iras}$	1.21	$0.98 < b_{\rm iras} < 1.56$
	Derived parameters	
Ω_b	0.085	
σ_8	0.67	
$\sigma_{8,\rm iras}$	0.81	
Γ	0.15	
$\beta_{\rm iras}$	0.47	
Age (Gyr)	16.5	

Table 1: Parameter values at the joint optimum. For the free parameters the 68% confidence limits are shown, calculated for each parameter by marginalising the likelihood over the other variables.

	Q	h	$\Omega_{\rm m}$	$b_{\rm iras}$
Q	1.00	0.40	−0.46	−0.49
h	0.40	1.00	−0.82	−0.57
$\Omega_{\rm m}$	−0.46	−0.82	1.00	0.09
$b_{\rm iras}$	−0.49	−0.57	0.09	1.00

Table 2: Parameter correlation matrix at the joint optimum

Fan and Cen 1997), and is in line with recent supernovae results (Perlmutter et al. 1998). However, given the assumption of a flat universe, it requires a very high cosmological constant ($\Omega_\Lambda = 0.6$). Gravitational lensing measurements have constrained $\Omega_\Lambda < 0.7$ (Kochanek 1996, Falco, Kochanek & Munoz 1998). Our value for the Hubble constant, $h = 0.53$, agrees well with several other measurements (Sugiyama 1995, Lineweaver et al. 1997), but falls at the low end of the generally accepted range from local measurements (Freedman et al. 1994). Assuming the nucleosynthesis constraint $\Omega_b h^2 = 0.024$ (Tytler, Fan & Burles 1996, Steigman, Hata & Felten 1998), the optimal baryon density is found to be $\Omega_{\rm b} = 0.085$. Our value for the combination $\sigma_8 {\Omega_{\rm m}}^{0.6} = 0.38$ is lower than the one derived from measurements from the peculiar velocity field, $\sigma_8 {\Omega_{\rm m}}^{0.6} \approx 0.8$ (Freudling et al. 1998). Our values are closer to the combination derived from cluster abundance $\sigma_8 {\Omega_{\rm m}}^{0.5} \approx 0.5$ (Eke, Cole & Frenk 1996, Bahcall, Fan and Cen 1997). Finally, for spatially-flat universes the time since the Big Bang for the values of our $\Omega_{\rm m}$ and h at the joint optimum is 16.5 Gyr.

On the IRAS side, $\beta_{\rm iras} = 0.47$ is in agreement with several other measurements (Strauss 1989, Schlegel 1995, Willick et al. 1997), although there are other measurements which place $\beta_{\rm iras}$ much higher (Dekel et al. 1993, Sigad et al. 1998). Willick et al. 1997 discuss the discrepancies between the various measurement techniques, and why they lead to such distinct results. Finally, the IRAS mass-to-light bias is seen to be slightly greater than unity ($b_{\rm iras} = 1.21$), suggesting that the IRAS galaxies (mainly spirals) are reasonable (but not perfect) tracers of the underlying mass distribution. We also note that our joint IRAS+CMB optimal values for $\sigma_{8,{\rm iras}}, \beta_{\rm iras}$ and Γ (Table 1) are in perfect agreement with the values derived from IRAS alone (FSL, Fisher 1994). However at fixed $\sigma_{8,{\rm iras}} = 0.69$ based on the IRAS correlation function FSL found a higher $\beta_{\rm iras} = 0.94 \pm 0.17$ and $\Gamma = 0.17 \pm 0.05(1 - \sigma)$. We emphasise that the naive linear biasing should be generalised to more realistic scenarios (e.g. Dekel and Lahav 1998).

As discussed in Section 5, the total CMB+IRAS reduced χ^2 at the joint optimum is 1.16, indicating that the optimum model is a good fit to both data-sets. We may compare this value with that obtained by Gawiser & Silk 1998. Using several data-sets Gawiser & Silk 1998 found the reduced χ^2 for ΛCDM to be 1.9, as opposed to a value of 1.2 for their 'best' model of Cold+Hot Dark matter (CHDM). However, using only the CMB and IRAS χ^2 values for ΛCDM in their Table 3, the total reduced χ^2 is found to be 1.00 as compared to a value of 0.95 for CHDM. Thus, using only the CMB and IRAS data-sets, ΛCDM is found to fit the observations as well as CHDM, and the results quoted by Gawiser & Silk 1998 are consistent with those presented here.

The near future will see a dramatic increase in LSS data (e.g. the PSCZ, SDSS, 2dF surveys) and detailed measurements of the CMB fluctuations on sub-degree scales (e.g. from the Planck Surveyor and MAP satellites). These will allow more accurate parameter estimation and the untying of the various parameters held fixed in the present work.

Acknowledgments

We would like to thank E. Gawiser, J. Felten, J. Silk, G. Steigman, K. Wu and I. Zehavi for helpful discussions. Matthew Webster and Sarah Bridle acknowledge PPARC studentships. Graça Rocha acknowledges a NSF grant EPS-9550487 with matching support from the State of Kansas and from a K*STAR First award.

REFERENCES

Bagla, J., S., 1998, MNRAS, in press, astro-ph/9711081)

Bahcall N.A., Fan, X., & Cen, R. 1997, ApJ, 485, L53

Baker J.C. et al. , 1998, MNRAS, submitted

Bardeen J.M., Bond J.R., Kaiser N. & Szalay A.S., 1986, ApJ, 304, 15

Bennett C.L. et al. , 1996, ApJ., 464, L1

Blanton, M., Cen, R., Ostriker, J.P., & Strauss, M.A., 1998, astro-ph/9807029

Bond J.R., 1995, *Cosmology and Large Scale Structure* ed. Schaeffer, R. Elsevier Science Publishers, Netherlands, Proc. Les Houches School, Session LX, August 1993

Bond J.R., 1995, Astrophys. Lett. and Comm., 32, 63

Bond J.R., Davis R.L. & Steinhardt P.J., 1995, Astrophys. Lett. and Comm., 32, 53

Carroll S.M., Press W.H. & Turner E.L., 1992, Ann. Rev. Astron. & Astrophy., 30, 499

Cheng E.S. et al. , 1994, ApJ., 422, L37

Cheng E.S. et al. , 1996, ApJ., 456, L71

Cole S., Fisher K.B. & Weinberg D.H., 1995, MNRAS, 275, 515

De Bernardis P. et al. , 1994, ApJ., 422, L33

Dekel A., Bertschinger E., Yahil A., Strauss M., Davis M. & Huchra J., 1993, ApJ, 412, 1

Dekel, A. & Lahav, O., submitted to ApJ, astro-ph/9806193

Efstathiou G., Bond J.R. & White S.D.M., 1992, MNRAS, 258, P1

Eisenstein, D.J., Hu, W. & Tegmark, M., 1998, astro-ph/9807130

Eke, V.R., Cole, S., and Frenk, C.S., 1996, MNRAS, 282, 263

Falco, E.E, Kochanek, C.S. & Munoz, J.A., 1998, ApJ, 494, 47

Fisher, K.B., in proceedings of 'Cosmic Velocity Fields', Paris, eds. Bouchet et al., pg. 177, Editions Frontieres

Fisher, K.B., Scharf, C.A. & Lahav, O., 1994, MNRAS, 266, 219

Fisher, K.B., Huchra, J.P., Strauss, M.A., Davis, M., Yahil A., Schlegel D., 1995, ApJ, 100, 69

Fisher K.B. & Nusser A., 1996, MNRAS, 279, L1

Freedman W., et al. , 1994, Nature, 371, 757

Freudling et al., 1998, submitted to ApJ

Gawiser E., & Silk J., 1998, Science, 280, 1405

Gundersen J.O et al. , 1995, ApJ., 443, L57

Gutierrez C.M., 1997, ApJ., 483, 51

Hancock S., et al. , 1994, Nature, 367, 333

Hancock S., Gutierrez C.M., Davies R.D., Lasenby A.N., Rocha G., Rebolo R., Watson R.A., Tegmark M., 1997, MNRAS, 298, 505

Hancock S., Rocha G., Lasenby A.N., Gutierrez C.M., 1998, MNRAS, 294, L1

Heavens A.F. & Taylor A.N., 1995, MNRAS, 275, 483

Kaiser N., 1987, MNRAS, 227, 1

Kaiser N., Efstathiou G., Ellis R., Frenk C., Lawrence A., Rowan-Robinson M., Saunders W., 1991, MNRAS, 252, 1

Kochanek C.S., 1996, ApJ, 466, 638

Lahav, O., Fisher, K.B., Hoffman, Y., Scharf, C.A, & Zaroubi, S., 1994, ApJL, 423, L93

Lahav O., 1996, Helv. Phys. Acta, 69, 388

Leitch E.M., Readhead A.C.S., Pearson T.J., Myers S.T., & Gulkis S., 1998, astro-ph/9807312

Lineweaver C.H., Barbosa D., Blanchard A. & Bartlett J.G., 1997, Astron. & Astrophy., 322, 365

Netterfield C.B., Devlin M.J., Jarosik N., Page L., Wollack E.J., 1997, ApJ, 474, 47

Peebles, P.J.E., 1980, *The Large-Scale Structure of the Universe*, (Princeton: Princeton University Press)

Pen, U.-L., 1998, astro-ph/9711180

Perlmutter S., et al. , 1998, Nature, 391, 51

Platt S.R., Kovac J., Dragovan M., Peterson J.B., & Ruhl J.E., 1997, ApJ, 475, L1

Press, W.H., Teukolsky, S.A., Vetterling, W.T., & Flannery, B.P., 1992, *Numerical Recipes (Second Edition)* (Cambridge: Cambridge University Press)

Rocha, G., Hancock, S., Lasenby, A.N., & Gutierrez, C.M. in preparation.

Ruhl J.E., Dragovan M., Platt S.R., Kovac J., & Novak G., 1995, ApJ., 453, L1

Scaramela N., & Vittorio N., 1990, ApJ., 353, 372

Scaramela N., & Vittorio N., 1993, ApJ., 411, 1

Schlegel D., 1995, Ph. D. Thesis, University of California, Berkeley

Scott D., Srednicki M., & White M., 1994, ApJ., 241, L5

Scott, P.F. et al. , 1996, ApJ., 461, L1

Seljak U., & Zaldarriaga M., 1996, ApJ, 469, 437

Sigad Y., Dekel A., Strauss M.A. & Yahil A., 1998, 495, 516

Smoot, G.F. et al. , 1992, ApJ., 396, L1

Steigman, G., Hata, N. & Felten, J.E., 1998, astro-ph/9708016

Strauss M.A., Ph. D. Thesis, University of California, Berkeley

Strauss, M.A., & Willick, J.A., 1995, Phys Rev, 261, 271

Sugiyama N., 1995, ApJ Supp., 100, 281

Tanaka, S.T. et al. , ApJ, 468, L81

Tegmark, M., & Peebles, P.J.E. 1998, astro-ph/9804067

Tytler D., Fan X.M. & Burles S., 1996, Nature, 381, 207

White et al. , 1993, Nature, 366, 429

Willick J.A., Strauss M.A., Dekel A. & Kolatt T., 1997, ApJ, 486, 629

Yahil, A., Strauss, M.A., Davis, M., & Huchra, J.P., 1991, ApJ, 372, 380

This preprint was prepared with the AAS LaTeX macros v4.0.

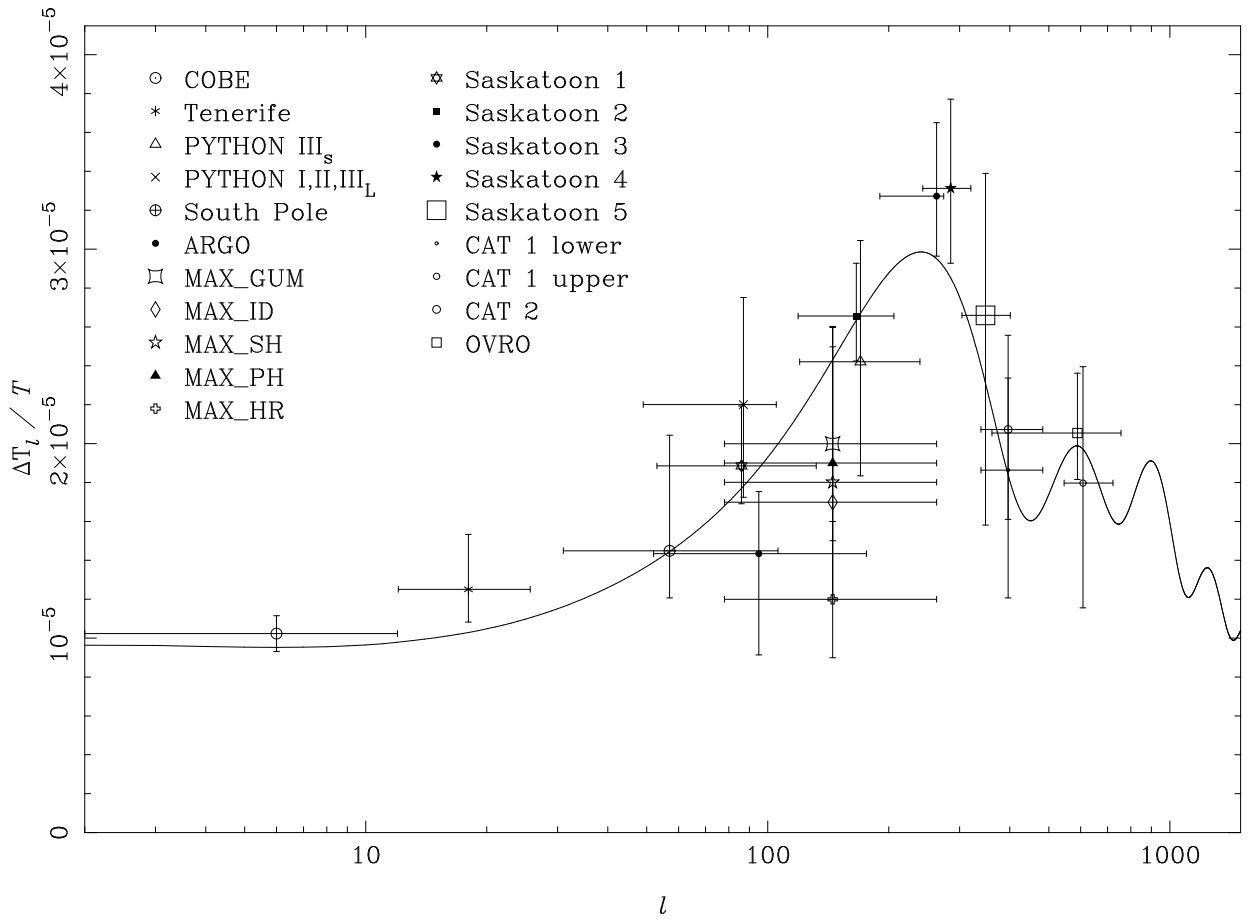

Fig. 1.— The data points used in the calculation of the CMB likelihood function. The overlaid curve is a model evaluated with optimal parameters shown in Table 1.

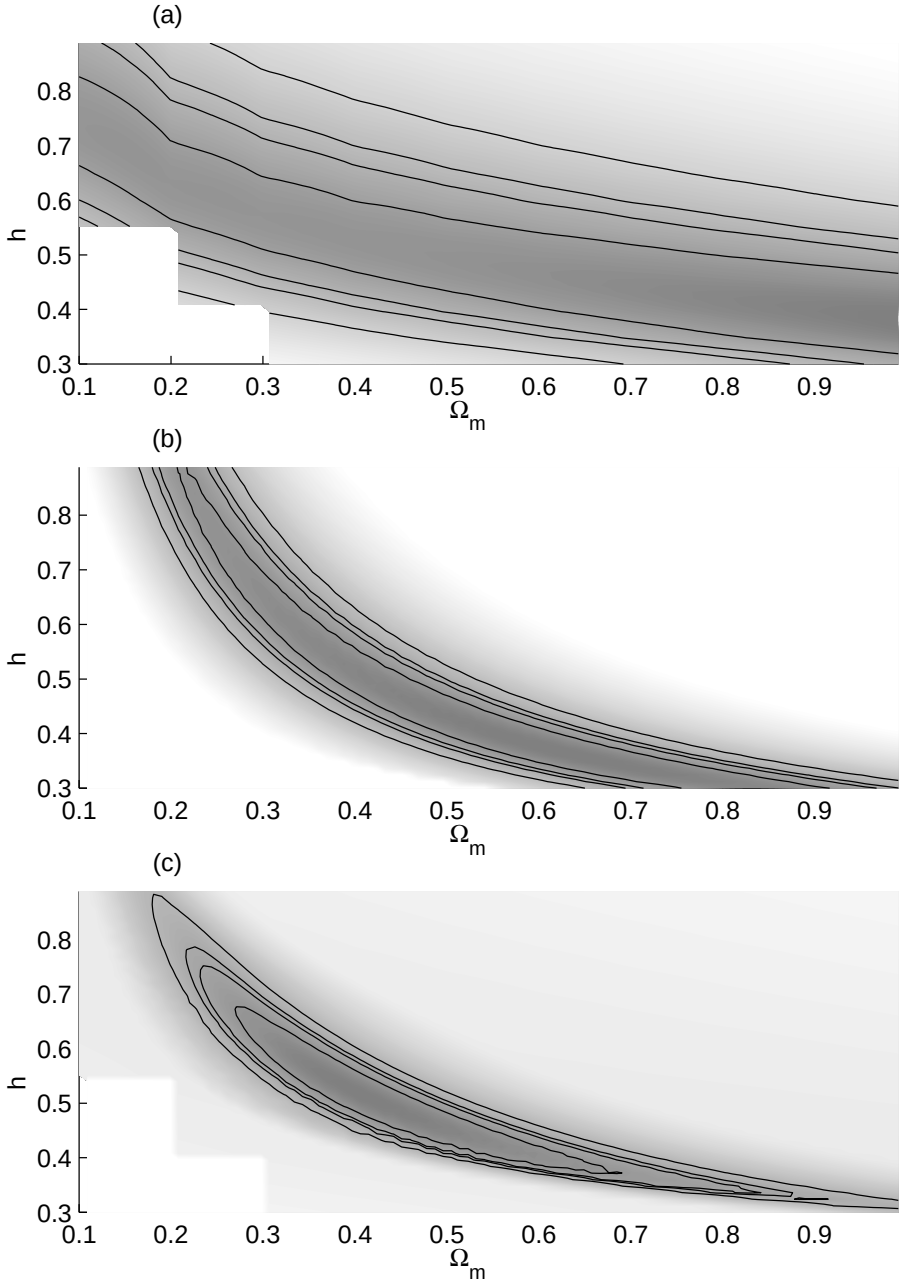

Fig. 2.— The likelihood function in the $\{\Omega_{\rm m}, h\}$-plane, after marginalisation over Q and $b_{\rm iras}$, for (a) CMB alone, (b) IRAS alone and (c) joint CMB and IRAS. The contours denote the 68, 90, 95 and 99 per cent confidence regions.

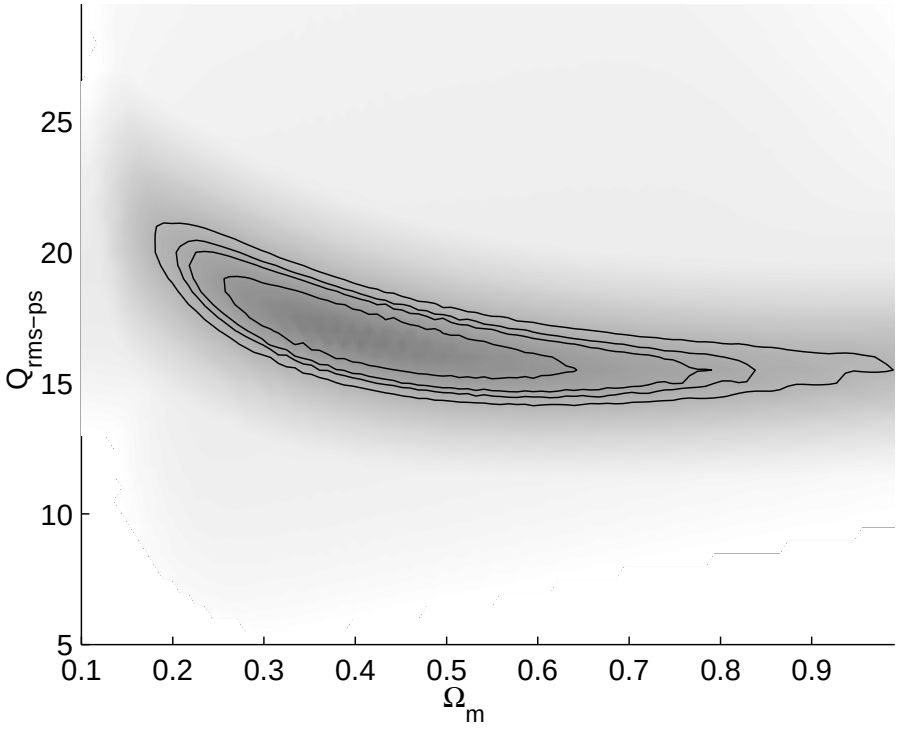

Fig. 3.— The joint CMB+IRAS likelihood function in the $\{\Omega_{\rm m},\, Q\}$-plane after marginalisation over h and $b_{\rm iras}$. The contours denote the 68, 90, 95 and 99 per cent confidence regions.

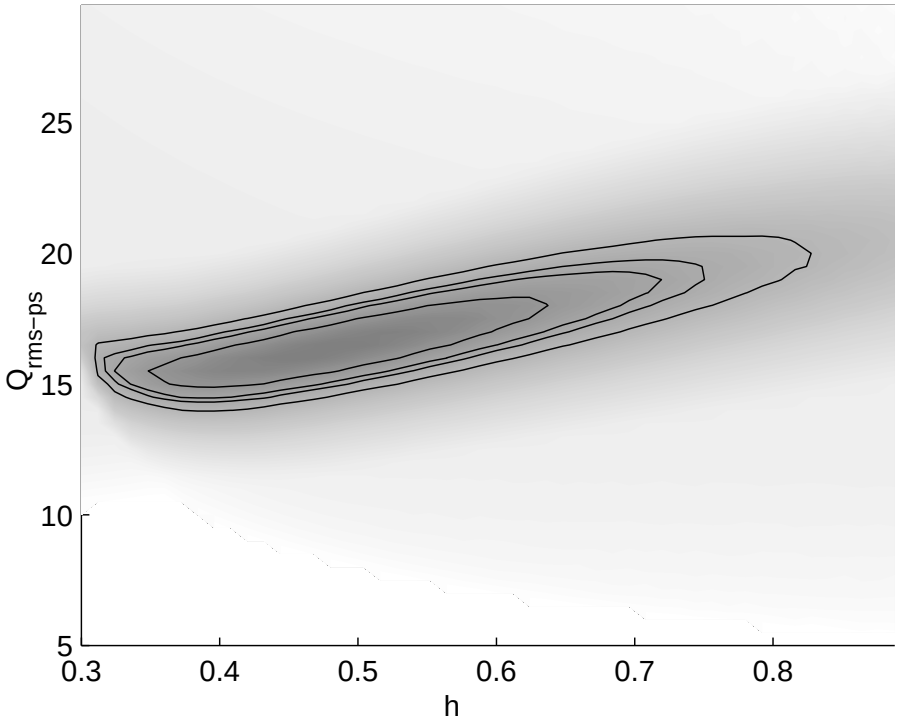

Fig. 4.— The joint CMB+IRAS likelihood function in the $\{h, Q\}$-plane after marginalisation over $\Omega_{\rm m}$ and $b_{\rm iras}$. The contours denote the 68, 90, 95 and 99 per cent confidence regions.

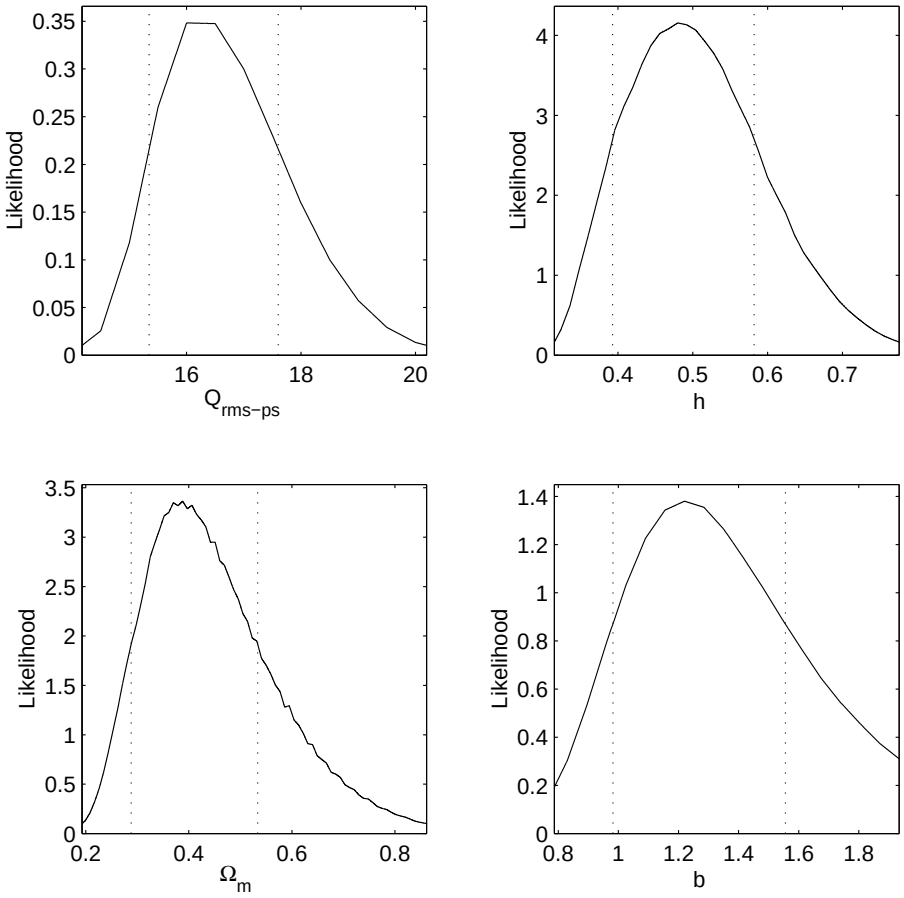

Fig. 5.— The one-dimensional marginalised probability distributions for each of the four parameters. The vertical dashed lines denote the 68% confidence limits. The horizontal plot limits are at the 99% confidence limits.